

1 **Upper Devonian mercury record from North America**
2 **and its implications for the Frasnian–Famennian mass**
3 **extinction**

4 **Zeyang Liu^{1,2,3}, Lawrence M. E. Percival⁴, Delphine Vandeputte⁴, David Selby^{3,5},**
5 **Philippe Claeys⁴, D. Jeffrey Over⁶, Yue Gao⁴**

6 ¹State Key Laboratory of Organic Geochemistry, Guangzhou Institute of
7 Geochemistry, Chinese Academy of Sciences, Guangzhou 510640, China

8 ²CAS Center for Excellence in Deep Earth Science, Guangzhou, 510640, China

9 ³Department of Earth Sciences, University of Durham, Durham DH1 3LE, UK

10 ⁴Analytical, Environmental and Geochemistry Group, Vrije Universiteit Brussel,
11 Pleinlaan 2, 1050 Brussels, Belgium

12 ⁵State Key Laboratory of Geological Processes and Mineral Resources, School of Earth
13 Resources, China University of Geosciences, Wuhan, 430074, Hubei, China

14 ⁶Department of Geological Sciences, SUNY College at Geneseo, Geneseo, NY 14454,
15 USA

16 Corresponding author: Zeyang Liu (geozy.liu@outlook.com)

17 Lawrence M. E. Percival (Lawrence.Percival@vub.be), Delphine Vandeputte

18 (Delphine.Jenny.Vandeputte@vub.be), Philippe Claeys (phclaeys@vub.be),

19 D. Jeffrey Over (over@geneseo.edu), Yue Gao (Yue.Gao@vub.be)

20 **Abstract**

21 The Frasnian–Famennian biotic crisis (~372 Ma) was one of the “big five” mass
22 extinction events in the Phanerozoic. This event was associated with dramatic climatic
23 and oceanographic perturbations, including oceanic anoxia, global cooling, sea-level
24 fluctuations, etc. Large-scale volcanic activity is one of several possible triggers that
25 have been suggested as the ultimate cause of this crisis, based on Hg enrichment data
26 from widespread sections. However, there are also sections that do not show a Hg
27 enrichment across the Frasnian–Famennian boundary. To further investigate the
28 hypothesis of a volcanic trigger for the Frasnian–Famennian mass extinction event,
29 mercury (Hg) analyses were performed on six North American records (five from the
30 Appalachian Basin and one in the Illinois Basin) that include the Frasnian–Famennian
31 boundary. There is no uniformly observed Hg enrichment at or below the Frasnian–
32 Famennian boundary across the six sites. A potentially volcanically driven Hg anomaly
33 is found in the Illinois basin; however, the Hg enrichment occurs stratigraphically
34 above the Frasnian–Famennian boundary. Mercury records from the studied sites
35 question the timing of the volcanism that may be responsible for the mass extinction
36 event. Further studies are needed to fully understand the geographic distribution and
37 eruption history of the large igneous provinces, as well as the link between Hg and
38 volcanism during the Frasnian–Famennian interval.

39 **Keywords:** Appalachian basin; Illinois basin; volcanism; large igneous provinces;
40 wildfires

41 **1. Introduction**

42 The Late Devonian Frasnian–Famennian (F–F) mass extinction (also known as the
43 Upper Kellwasser Crisis, ~372 Ma; Becker et al., 2012; Da Silva et al., 2020; Percival
44 et al., 2018a), is one of the ‘big five’ mass extinction events of the Phanerozoic Eon
45 (Stanley, 2016). Marine ecosystems, especially metazoan reefs, were severely impacted
46 during this biotic crisis (Ma et al., 2016; Stanley, 2016). Stratigraphic records of the
47 extinction are associated with a large positive carbon-isotope excursion (up to 4 ‰)
48 both in the inorganic and organic carbon contents ($\delta^{13}\text{C}_{\text{carb}}$ and $\delta^{13}\text{C}_{\text{org}}$) of sedimentary
49 strata in the *linguiformis* conodont Zone (= Frasnian Zone 13b) across the globe,
50 indicating perturbations to the carbon cycle beginning ~150 kyr prior to the end of the
51 Frasnian Stage (e.g., Chen et al., 2005; De Vleeschouwer et al., 2017; Joachimski and
52 Buggisch, 1993; Joachimski et al., 2002; Stephens and Sumner, 2003; Wang et al.,
53 1996). Proposed causes of the F–F mass extinction event include globally anoxic or
54 euxinic marine conditions (Bond et al., 2004; Song et al., 2017), land-plant evolution
55 (Algeo et al., 1995), climate cooling (Huang et al., 2018; Joachimski et al., 2009;
56 Joachimski and Buggisch, 2002), sea-level change (Bond and Wignall, 2008; Johnson
57 et al., 1985), bolide impact (Claeys et al., 1992) and volcanism (e.g., Racki, 2020; Racki
58 et al., 2018b). Recently, the volcanism scenario has been supported by the discovery of
59 spikes in mercury (Hg) concentrations at several F–F boundary records (Estrada et al.,
60 2018; Moreno et al., 2018; Racki et al., 2020; Racki et al., 2018a; Racki et al., 2018b;
61 Kaiho et al., 2021). Mercury and its isotopes have been used as a marker of ancient

62 volcanic events associated with several other major climate perturbations and/or
63 extinctions in the geological history, such as the Permian–Triassic mass extinction,
64 Toarcian Ocean anoxic event, Late Ordovician mass extinction, Paleocene–Eocene
65 thermal maximum, and end-Devonian mass extinction, etc. (e.g., Grasby et al., 2016;
66 Grasby et al., 2020; Grasby et al., 2013; Grasby et al., 2017; Grasby et al., 2019; Jones
67 et al., 2018; Liu et al., 2019a; Percival et al., 2018b; Percival et al., 2015; Paschall et
68 al., 2019; Sanei et al., 2012; Shen et al., 2019a; Shen et al., 2019b; Them et al., 2019;
69 Kaiho et al., 2020, 2021). Volcanic events can emit mercury through two pathways: (1)
70 direct outgassing from effusive and explosive volcanic eruptions, and (2) Hg-enriched
71 volatiles that are hypothesized to have been generated by contact metamorphism of
72 organic-rich sedimentary rocks and subsequently emitted through hydrothermal vent
73 complexes (Jones et al., 2019). In either case, the emitted Hg is distributed far from the
74 source through the atmosphere, due to a relatively long stratospheric residence time of
75 around 0.5–2 years (e.g. Driscoll et al., 2013). In modern environments, mercury is
76 typically deposited to sediments complexed with organic matter (Gamboa Ruiz and
77 Tomiyasu, 2015; Gehrke et al., 2009; Outridge et al., 2007; Sanei et al., 2014). Thus,
78 normalization against TOC is necessary to evaluate whether any Hg enrichment is
79 caused by increased organic matter preservation or an externally derived influx of the
80 element during perturbations of the local/global Hg cycle. In addition to organic matter,
81 clay minerals and sulphides may also be important host fractions within the sediments
82 (Grasby et al., 2019; Shen et al., 2019a, 2020). However, in spite of global-scale records

83 of Hg enrichment at the Frasnian–Famennian boundary, some sections do not show a
84 trend of Hg enrichment (Racki et al., 2019). Thus, the timing and magnitude of the
85 volcanism that may be responsible for the Frasnian–Famennian biotic crisis is still
86 poorly understood.

87 In addition to volcanism, local/global Hg cycling may also be perturbed by the
88 disruption of terrestrial Hg sources, such as wildfires and continental runoff (e.g. Amos
89 et al., 2014; Biswas et al., 2007; Sanei et al., 2012; Them et al., 2019; Grasby et al.,
90 2017; Shen et al., 2019c). Forests and organic-rich upper soils are major terrestrial Hg
91 pools (e.g., Obrist et al., 2018); thus, biomass burning would release Hg back into the
92 atmosphere and volatile Hg that stored in organic-rich soils (Obrist et al., 2018). The
93 amount of Hg released from wildfire would, of course, depend on the quantity of plant
94 burning to some degree. The burning severity is also an important factor controlling the
95 degree of Hg emission from wildfires (Webster et al., 2016). The higher the burning
96 temperature, the greater the emissions of Hg from soil heating (Webster et al., 2016). It
97 has also been suggested that Hg emissions from post-fire soil erosion could represent a
98 significant Hg source to the oceans and atmosphere (Melendez-Perez et al., 2014).

99 Finally, terrestrial runoff can also act as an important contributor to the Hg budgets
100 of the oceans (Fisher et al., 2012; Soerensen et al., 2012). The majority of Hg is bound
101 to organic matter particles in the river and deposited in deltas, estuaries and on the
102 continental shelf (Chester, 1990). Thus, riverine Hg discharges largely affect nearshore
103 Hg sediments, as supported by the Hg-isotopic compositions of nearshore *vs* more distal

104 marine sediments (e.g., Grasby et al. 2017; Shen et al., 2019). In the event of enhanced
105 continental weathering, riverine Hg input to the ocean would likely become more
106 significant (Grasby et al., 2017; Them et al., 2019). Although wildfires and riverine Hg
107 inputs are relatively well constrained in the modern Hg cycles (e.g., Amos et al., 2014;
108 Obrist et al., 2018), their role in ancient Hg records are still poorly understood due to
109 both a paucity of data (but see Grasby et al., 2017; Them et al., 2019), and, in the case
110 of the Devonian, a markedly different global paleogeography and terrestrial biosphere.

111 In this study, we perform mercury (Hg) analysis on six Frasnian–Famennian
112 boundary sections from North America (New York and Iowa). We discuss the potential
113 evidence for volcanic and terrestrial mercury emissions at the time of the Frasnian–
114 Famennian extinction, and, by inference, any potential volcanic link with that biotic
115 crisis. Of the investigated sections, the five New York sites comprise a proximal to
116 distal transect, and have been previously examined for wildfire records (Liu et al.,
117 2020a). As such, these sections are also ideal for the evaluation of wildfires and riverine
118 runoff (as well as volcanism) as sources of Hg input into the oceans in the geological
119 record.

120 **2. Geological background**

121 In this study, samples were collected from six Frasnian–Famennian archives of
122 North America (Fig. 1). Five records from western New York were investigated,
123 including four outcrop sections (Joint Creek, JC; Beaver Meadow Creek, BMC; Irish
124 Gulf, IG; Walnut Creek Bank, WCB), and one drill core (West Valley, WV). These

125 records are preserved as slope to basin deposits from the northern Appalachian foreland
126 basin, and are interpreted as proximal to distal deposits in terms of paleoceanography,
127 with the following order of increasing distance from the paleoshoreline: JC, BMC, WV,
128 IG and WCB (see inserted map of Fig. 1) (Over et al, 1997, 2002; Sageman et al., 2003).
129 In all five records, the studied interval is composed of the latest Frasnian–earliest
130 Famennian Hanover Formation and the early Famennian Dunkirk Formation. The
131 Hanover Formation is dominated by light gray, silty shales (less than 1 wt. % total
132 organic carbon, TOC) interbedded with black silty shales that is rich in organic matter
133 (~1–6 wt. % TOC) with low thermal maturity ($BR_o \sim 0.6\%$, solid bitumen reflectance;
134 Liu et al., 2020a). The grey shales are bioturbated, and poorly preserved brachiopods
135 and bivalves have been identified within it (Over, et al., 1997; Over, 2002). The black
136 shales are rich in pyrite and finely laminated (except the base parts where bioturbation
137 is observed), suggested that they were deposited in anoxic/dysoxic conditions (Lash,
138 2017; Over, et al., 1997; Over, 2002; Sageman et al., 2003). The Hanover Formation is
139 overlain by the Dunkirk Formation, which contains thick beds of black shale (Over, et
140 al., 1997). In all five Appalachian Basin records studied here, the F–F boundary is
141 defined by the first occurrence of the conodont *Palmatolepis triangularis* (Fig. 2;
142 Klapper et al., 1993; Over, 1997, 2002). This boundary occurs in a regionally
143 continuous bed of black shale that is thought to locally mark the Upper Kellwasser
144 Horizon (Over, 1997, 2002).

145 To obtain a more regional scale viewpoint beyond the local environment of the
146 Appalachian Basin, the H-32 drill core was studied as a sixth record, consisting of
147 sediments deposited in a deep-water environment of the Illinois Basin (40.47° N, 91.47°
148 W; Fig. 1; Day and Witzke, 2017). The Frasnian–Famennian interval in the Illinois
149 Basin is composed of the Sweetland Creek Shale Formation (shales and carbonates)
150 and the overlying Grassy Creek Shale Formation (fissile organic-rich brown shale). The
151 F–F boundary is positioned just above the base of the Grassy Creek Shale (above the
152 conodont Zones 13b and 13c; i.e., the *linguiformis* interval) (Fig. 3; De Vleeschouwer
153 et al., 2017). Several volcanic ash layers are also preserved in the lowermost part of
154 Grassy Creek Shale Formation, just above the F–F boundary (Fig. 3; De Vleeschouwer
155 et al., 2017).

156 **3. Methods**

157 Mercury (Hg) concentrations were determined on an Advanced Mercury Analyser
158 (AMA) 254.7 at Vrije Universiteit Brussel. Mercury in the solid sample was volatilized
159 during direct thermal decomposition of the sample, and the resultant gas drawn into an
160 amalgamator containing a gold trap, before being analyzed by atomic absorption
161 spectrometry (see Sholupov and Ganeyev, 1995). Blank measurements on the AMA
162 during the analyses were better than 0.001 ng. 100±2 mg of powdered sample was used
163 per analysis, with at least two measurements per sample to check repeatability, which
164 was typically better than ±10%. The accuracy and repeatability of the measurements

165 was further tested by multiple measurements of the Certified Reference Material IAEA-
166 MESL-ILC-TE and an internal sedimentary sample SCH U5 as standards.

167 Total organic carbon (TOC) contents and isotopic compositions of the TOC were
168 determined for samples from the H-32 core using a Nu Instruments Horizon 2 coupled to
169 an Eurovector isotope ratio mass spectrometer (IRMS) elemental analyzer EuroEA3000 at the
170 Vrije Universiteit Brussel (Belgium). Approximately 1–2 grams of homogenized powder were
171 decarbonated with 10% HCl, before being rinsed three times with mill-Q water and dried at 50
172 °C. Analyses of the decarbonated samples were calibrated using the international reference
173 materials IAEA-CH-6 (sucrose), and multiple certified reference materials that have been
174 calibrated against international standards: IA-R041 (L-alanine), IVA33802151 (organic-rich
175 sediment), IVA33802153 (organic-poor soil). The measured carbon content in decarbonated
176 powder was converted to a bulk rock TOC value by accounting for the measured mass lost
177 following decarbonation. Analytical uncertainty was typically better than ± 0.1 wt% (1σ) for
178 carbon contents, and ± 0.2 ‰ (1σ) for isotopic compositions.

179 **4. Results**

180 All the Hg analysis data are listed in Table S1 and S2, and the stratigraphic plots
181 are presented in Fig. 2 and Fig. 3.

182 At the Joint Creek section, the Hg concentrations are generally above 30 ppb
183 below the F–F boundary, dropping slightly to ~25 ppb at the base of the Dunkirk
184 Formation. The Hg/TOC values show a slight increase from ~20 ppb/wt.% at the

185 bottom part to ~26 ppb/wt.% towards the F–F boundary, which then decrease to ~20
186 ppb/wt.% at the base of Dunkirk Formation.

187 At the Beaver Meadow Creek section, the Hg values are generally about 20 ppb
188 in the lower part of the section, with an increase up to ~54 ppb about 15 cm below the
189 F–F boundary. The Hg values then drop to ~30 ppb immediately below the boundary
190 and further decline to ~20 ppb across it. Hg/TOC values also reach their maximum
191 about 15 cm below the F–F boundary (from ~10 to ~22 ppb/wt.%), dropping to less
192 than 10 ppb across the F–F boundary.

193 At the West Valley section, the Hg values range from ~22 to 43 ppb across the
194 studied intervals, with no clear pattern observed. The Hg/TOC values average about 35
195 ppb/wt.% (n = 6) at the lowest part of the section, which then decrease gradually to
196 about 11 ppb/wt.% around the F–F boundary and remain at ~10 ppb/wt.% up section,
197 except for one sample with an anomalously high Hg/TOC value (81.88 ppb/wt.%) that
198 is caused by low TOC level (0.32% compared to average 2.5% for adjacent samples).

199 At the Irish Gulf section, the Hg values drop from ~30 ppb to 15 ppb at the very
200 bottom part, which then rapidly increase to ~46 ppb around the F–F boundary. The Hg
201 values then decrease to about 25 ppb and further drop slightly to about 23 ppb upwards.
202 The Hg/TOC values drop gradually from ~12 ppb/wt.% to ~5 ppb/wt.% across the F–
203 F boundary and remain around 5 ppb/wt.% towards a higher stratigraphic level.

204 At the Walnut Creek Bank section, the Hg values increase from ~35 ppb to ~56
205 ppb across the F–F boundary, which then gradually drop to ~25 ppb at the base of the

206 Dunkirk Formation. Except for a very high Hg/TOC value of 51 ppb/wt.% at the bottom
207 of this section, samples below the F–F boundary generally have Hg/TOC values about
208 11 ppb/wt.%, which then gradually decrease to ~6 ppb/wt.% towards the lower part of
209 the Dunkirk Formation (Fig. 2).

210 In the H-32 core, the Hg values range from ~44 to 213 ppb (average ~98 ppb, n =
211 19), with several peaks at the bottom part of the section, which then gradually decrease
212 to a minimum of ~16 ppb just below the F–F boundary. The Hg values then increase
213 sharply to ~314 ppb immediately above the F–F boundary, before gradually declining
214 to ~46 ppb at the top of the studied interval. A minimum threshold of 0.2 wt.% TOC
215 has been suggested for normalization of Hg by TOC, in order to avoid artificially
216 inflated Hg/TOC spikes due to the high uncertainty/value ratio of the TOC data (Grasby
217 et al., 2016). A sharp rise in TOC content takes place just below the F–F boundary,
218 from typically <0.5 wt.% (apart from a discrete layer between 281–335 cm where
219 values rise to over 2 wt. %), to an average of 3.1 wt.% in the uppermost Frasnian and
220 Famennian strata (Fig. 3). This rise in TOC occurs at the base of the Grassy Creek Shale
221 Formation and within a broad rise in $\delta^{13}\text{C}_{\text{org}}$ values from -28.5 ‰ to -27.1 ‰, and is,
222 therefore, interpreted as marking the local expression of the Upper Kellwasser Horizon.
223 The Hg/TOC values average about 251 ppb/wt.% (n = 16) at the lower part of the
224 section, with two one-point excursions to 790 and 722 ppb/wt.%. The Hg/TOC values
225 then drop to ~200 ppb/wt.% below the F–F boundary, which then further drop to ~17
226 ppb/wt.% across the F–F boundary. A one-point excursion to 1127 ppb/wt.% is detected

227 above the F–F boundary, reflecting a low TOC value (0.2 %) of the sample compared
228 to the rocks either side that feature both high Hg and organic matter contents (Fig. 3).
229 Notably, both Hg and Hg/TOC values recorded in the H-32 core are significantly higher
230 than for the five Appalachian Basin records.

231 **5. Discussion**

232 *5.1 Constraining the Hg source(s)*

233 The Appalachian Basin sites have Hg values average 30.5 ppb (15.1 ppb/wt.%
234 Hg/TOC), which are relatively low compared to postulated average shale
235 concentrations (62.4 ppb Hg and 71.9 ppb/wt.% Hg/TOC; Grasby et al., 2019). Thus,
236 the majority of the samples (except the peaks in Hg documented from the H-32 core)
237 would also be classified as average shale contents (Fig. 3). This low Hg abundance does
238 not seem to result from dilution by a high sedimentation rate, as the formation of shale
239 generally requires a low sedimentation rate, and there is no discernible Hg abundance
240 difference between the WV and WCB sections where sedimentation rates could vary
241 by up to ~7 times (based on an appropriate estimation according to the thickness
242 between the F–F boundary and the base of the Dunkirk Formation). In addition to
243 organic matter, the Hg may also be associated with sulphides and clay minerals in
244 certain environments (Bergquist, 2017; Shen et al., 2019a; Shen et al., 2020; Them et
245 al., 2019). Thus, if mercury is deposited bound to one of those phases, it may cause a
246 rise in sedimentary Hg and Hg/TOC values without any major increase of the Hg fluxes
247 from its sources. However, Algeo and Liu (2020) compiled a large geochemical dataset

248 of trace-metal redox proxies and found that the Hg/TOC and Hg/S ratios of ancient
249 sediments were generally not significantly related to local redox conditions, and thus
250 might reflect volcanic Hg fluxes. A non-relationship between redox changes and
251 Hg/TOC ratios is also supported for the sites studied here by the lack of correlation
252 between Hg/TOC and redox proxies (Mn, Mo, $V/[V + Ni]$, Mo_{EF} , V_{EF} and Ni_{EF} ; Table
253 S1).

254 After normalization against the TOC data, only the Beaver Meadow Creek section
255 from western New York shows a minor Hg (Hg/TOC) enrichment below the F–F
256 boundary. No positive correlation between this Hg peak and Mo concentrations is
257 observed; indeed, the increase of Hg and Hg/TOC values is associated with a decrease
258 in Mo content (Fig. 2 and 4, Table S1, $r = +0.10$, $p(a) > 0.05$, $n = 52$). The Mo element
259 might be affected by changes of the marine reservoir size due to restriction of the
260 Appalachian Basin (Algeo, 2004). However, Hg and Hg/TOC values also lack
261 correlations with Mn and $V/(V+Ni)$ proxies (Fig. 4). This result suggests that the
262 mercury enrichment did not result from redox changes or a switch to burial with
263 sulphides. An increase of clay mineral content is also excluded for driving the Beaver
264 Meadow Creek Hg enrichment, as no linear relationship is observed between
265 sedimentary Hg and Al_2O_3 contents (Table S1; $r = +0.10$, $p(a) > 0.05$, $n = 52$).

266 Previous studies have suggested that wildfire activity could release Hg into the
267 environment (Biswas et al., 2007; Sanei et al., 2012; Them et al. 2019; Grasby et al.,
268 2017, 2019, and references therein). Fossilised charcoal, a by-product of wildfires, has

269 been widely used to study ancient fire events (e.g., Glasspool and Scott, 2010). A
270 previous organic petrology study of the New York sections found the presence of
271 fossilised charcoal (inertinite) as evidence for wildfire activity (Liu et al., 2020a).
272 However, no correlation between Hg concentration and inertinite abundance is
273 observed in this study (Fig. 2; Liu et al., 2020a). Although it is possible that wildfire-
274 released Hg and charcoal (inertinite) entailed different durations to reach the
275 depositional record, it would be expected that the majority of Hg and inertinite would
276 be deposited geologically simultaneously. During biomass burning, Hg is released from
277 plant combustion, as well as soil heating (Friedli et al., 2003; Obrist et al., 2007).
278 Thermal volatilization of the Hg bonded to the organic-rich soil would occur at 150 °C
279 (Biester and Scholz, 1996), with mercury readily emitted once the soil reached that
280 temperature (Biswas et al., 2007, 2008; Woodruff and Cannon, 2010). Previous
281 charcoal-reflectance analyses have suggested that the type of wildfire documented in
282 the New York F–F records was surface fire, with a burning temperature between 400
283 and 500 °C (Liu et al., 2020a). The primary burnt material was herbaceous and shrubby
284 plant matter (Liu et al., 2020a), and it is possible that such plants do not sequester Hg
285 efficiently. However, previous research has suggested that the temperature of burning
286 is different from that of soil heating due to a strong thermal gradient. Thus, a fire with
287 burning temperature of 850 °C on the surface would generally not increase the
288 subsurface temperature over 150 °C below 5 cm (Debano, 2000). If this was also the
289 case for wildfires during the F–F extinction, it might explain the apparent lack of Hg

290 emissions from soil heating at that time. Alternatively, the wildfires may have been too
291 small in scale (with a low burning severity), or the ash and charcoal have too low a Hg
292 content, to supply large amounts of mercury to the local environment. Kaiho et al.
293 (2021) report Hg/TOC enrichments together with coronene spikes are shown for three
294 carbonate-dominated F-F sections (Yangdi, China; Sinsin, Belgium; Coumiac, France;
295 with TOC generally less than 0.3 %), and concluded that the Hg was emitted from
296 thermal heating of country rocks by sill intrusion, rather than normal wildfire, as
297 supported by the evidence of coronene index [coronene/(benzo[e]pyrene +
298 beozo[ghi]perylene + coronene)] (Kaiho et al., 2016, 2020, 2021). Whilst coronene
299 requires higher energy to form than other polycyclic aromatic hydrocarbons (PAHs), a
300 higher energy demand cannot rule out the wildfire origin of coronene. Additionally,
301 there are also further factors that may affect the PAHs compositions (e.g. burning
302 pattern, plant community etc.; Boudinot and Sepúlveda, 2020; Lima et al., 2005). In
303 addition, most samples have coronene index over the threshold of 0.2 in the studied
304 sections (which would suggest coronene generated from heating by sill intrusion or
305 wildfires set by high temperature magma, in contrast to normal wildfires, according to
306 the authors), and this would imply a prolonged time duration for the volcanism, which
307 is unlikely and does not correlate with the Hg/TOC profiles. We suggest that it is still
308 at an early stage to link the coronene spikes with magmatic activity and interpret the
309 Hg/TOC as a signal of volcanism and associated volatilization of mercury from
310 organic-rich sediments by sill intrusions. Importantly, other events for which sill

311 intrusions of organic-rich shales have been proposed invariably feature a pronounced
312 negative carbon-isotope excursion (assumed to reflect the large-scale release of
313 isotopically light carbon from the intruded lithologies; e.g., Svensen et al., 2004, 2009;
314 McElwain et al., 2005), in contrast to the positive $\delta^{13}\text{C}$ shift that marks the F–F
315 boundary.

316 Riverine discharge of Hg to the oceans is another important source and may
317 significantly affect the Hg record of the proximal sections (e.g., Amos et al., 2014 and
318 many others). In theory, if riverine input is the controlling factor of Hg enrichment, a
319 trend of decreasing Hg concentrations from proximal to distal transections might be
320 expected (see Them et al., 2019). However, no such relationship is found within the
321 five Appalachian Basin sections. Rather, the most distal sections have the highest
322 average Hg abundance (from proximal to distal: Joint Creek–29.5 ppb, Beaver Meadow
323 Creek–30.8 ppb, West Valley–29.7 ppb; Irish Gulf–28.1 ppb; Walnut Creek Bank–
324 35.32 ppb). We have also noted that the four proximal sections have very similar
325 average Hg concentrations, despite variable TOC amounts (from proximal to distal:
326 Joint Creek–1.37 %, Beaver Meadow Creek–2.33 %, West Valley–2.10 %; Irish Gulf–
327 3.40 %). As such, our data suggest that riverine Hg input and organic matter
328 sequestration played minimal roles in the Hg enrichment within the Appalachian Basin.
329 However, it is also possible that the studied sites are too geographically close to yield
330 any noticeable difference on the Hg records, as evidenced by similar Ti/Al values of
331 these sections (Fig. 1, Table S1).

332 Racki (2020) proposed a hypothesis of masked signal of Hg in Devonian records,
333 i.e., a co-increase of productivity and Hg abundance may keep the Hg/TOC values
334 constant, or even reduce the Hg/TOC values if the percentage increase of organic matter
335 preservation is higher than the amount of Hg increase, as has also been proposed for
336 some Mesozoic events (see Percival et al., 2015, 2018b; Charbonnier and Föllmi,
337 2017). However, for the western New York sites, increases in both Hg and Hg/TOC are
338 largely absent, suggesting that there was no major increase in mercury input to this
339 region, rather than a volcanic influx that was then masked by elevated TOC. The
340 variations of the Hg data in western New York sections are more appropriately
341 explained by a combination of local depositional factors. In summary, the western New
342 York sections show no major perturbations of the Hg cycle that may be linked with
343 volcanic events. Variations of local depositional factors are more likely to be the main
344 control of the Hg fluctuations at western New York sections.

345 Two Hg/TOC spikes (up to ~800) are detected about 4–6 m below the F–F
346 boundary in the H-32 core (Fig. 3). These Hg enrichments are well above the
347 background the Hg/TOC values, suggesting a potential volcanic contribution or local
348 environmental perturbation (e.g., sulphides depositions), although currently the exact
349 roles of clay mineral and sulphides are not evaluated due to a paucity of data. However,
350 these peaks are about 750–900 kyr before the mass extinction event (De Vleeschouwer
351 et al., 2017). Consequently, even if those Frasnian Hg/TOC peaks are indicative of

352 large-scale volcanic eruptions, they likely occurred too early to have triggered the mass
353 extinction event.

354 We have also noticed that both the H-32 core and the West Valley section express
355 a single-point Hg/TOC peak above the F–F boundary (Fig. 2 and 3), although there is
356 no evidence as to whether these enriched strata are time equivalent. However, these
357 Hg/TOC spikes are not likely caused by enhanced Hg input from volcanism, due to
358 their apparent correlation to a TOC minimum in those intervals (Fig. 2 and 3). The H-
359 32 core does document large-scale Hg perturbations from less than 100 ppb to over 300
360 ppb above the F–F boundary, but the Hg/TOC values generally remain relatively
361 constant. Thus, these strata could simply record an increase in organic matter burial
362 under anoxic–euxinic conditions, and a resultant rise in Hg deposition. Intriguingly
363 however, this increase in Hg content correlates with the lowermost Famennian volcanic
364 ash layers preserved in the H-32 core (Fig. 3), potentially indicating volcanism as an
365 Hg source that was muted by excess organic-matter deposition, (Fig. 3; cf. Racki,
366 2020). This scenario would match the model of Racki (2020), but even if this was the
367 case, this volcanism occurred after the F–F extinction, and cannot have triggered the
368 event.

369 *5.2 No Hg evidence in North America for a volcanic trigger of the F–F mass extinction*

370 A volcanic trigger has long been proposed to have caused the F–F mass extinction
371 (e.g., Courtillot et al., 2010; Kravchinsky, 2012; Racki et al., 2002). Recently, this
372 scenario has been supported by the discovery of widely distributed Hg anomalies in the

373 F–F stratigraphic interval (Estrada et al., 2018; Moreno et al., 2018; Racki et al., 2020;
374 Racki et al., 2018a; Racki et al., 2018b), although some localities do not show a Hg
375 enrichment signal (Racki et al., 2019). In this study, among the five sections
376 investigated in western New York, only one section (Beaver Meadow Creek) expresses
377 a Hg and Hg/TOC peak below the F–F boundary (Fig. 2), but it is too small in scale to
378 be unequivocally linked with volcanism rather than local depositional processes, and
379 may simply result from a combination of changes in local depositional environments,
380 such as redox variation, organic matter preservation, sulphide precipitation and clay
381 mineral input. The H-32 section in Iowa shows a major Hg enrichment (from 58 to 314
382 ppb), which is correlative with volcanic ash layers, but this Hg peak is above the F–F
383 boundary (Fig. 2 and 3), and is largely correlative with elevated TOC contents. Even if
384 the H-32 peak was associated with volcanism, it remains unclear whether it was linked
385 to local eruptions that produced the ash layers, or a large-scale magmatic event (e.g.,
386 Viluy Traps, Kola, Vyatka, and Pripyat-Dniepr-Donets rift systems; Arzamastsev et al.,
387 2017; Kiselev et al., 2006; Kravchinsky, 2012). However, a correlation between
388 individual eruptive events and stratigraphic Hg enrichments has been speculated for
389 other sites, and increased arc activity also postulated as a trigger for the F–F extinction
390 (Racki et al., 2018; Racki, 2020).

391 The osmium-isotope ratio of a sedimentary rock is another widely used proxy to
392 study ancient volcanic events (e.g., Dickson et al., 2015; Du Vivier et al., 2014;
393 Georgiev et al., 2015; Liu et al., 2020b; Liu et al., 2019b; Percival et al., 2020; Peucker-

394 Ehrenbrink and Ravizza, 2012; Turgeon and Creaser, 2008). The modern seawater
395 osmium-isotope ($^{187}\text{Os}/^{188}\text{Os}$) composition is controlled by the mass balance of
396 unradiogenic Os input from mantle and extraterrestrial sources (~ 0.126) and riverine
397 input of radiogenic material following weathering of ancient continent crust (~ 1.4
398 today) (Peucker-Ehrenbrink and Ravizza, 2000). In the event of large-scale volcanism
399 and/or weathering of newly emplaced volcanic basalts, a shift in the Os-isotope profile
400 to lower values would be expected (e.g., Du Vivier et al., 2014; Georgiev et al., 2015;
401 Liu et al., 2019b; Turgeon and Creaser, 2008). However, available Os-isotope data for
402 the F–F transition interval do not show a clear unradiogenic shift, although a few data
403 points do have quite unradiogenic values of ~ 0.2 and 0.3 (Gordon et al., 2009; Liu et
404 al., 2020a; Percival et al., 2019; Turgeon et al., 2007). Thus, if volcanism indeed
405 occurred at this time, it is likely to be a small/transient event that differs from other
406 LIPs claimed to be responsible for major environmental/biotic perturbations. For
407 example, LIP activity associated with the Late Cretaceous Cenomanian–Turonian
408 Oceanic Anoxic Event lasted ~ 200 kyr and is marked by a global-scale shift to very
409 unradiogenic values in the sedimentary Os isotope record (e.g., Du Vivier et al., 2014,
410 2015; Percival et al., 2020; Jones et al., 2020). Prolonged unradiogenic Os isotope shifts
411 are also documented in response to widespread igneous activity related to the Central
412 Atlantic magmatic province during the Triassic–Jurassic boundary interval (Cohen and
413 Coe, 2002; Kuroda et al., 2010).

414 Instead, an increase in Os isotope values has been reported from the Kowala
415 Quarry section (Poland), and interpreted to reflect enhanced weathering of the continent
416 (Percival et al., 2019). Although this same signal has not been reported from the New
417 York Sites (Turgeon et al., 2007; Gordon et al., 2009; Liu et al., 2020a), it should be
418 noted that those osmium records focus on the F–F boundary itself, whereas the Kowala
419 weathering peak is just below the base of the Upper Kellwasser Level, which is
420 typically somewhat stratigraphically below the F–F horizon, and thus may not have
421 been reached by the New York datasets. However, a weathering signal in Os isotopes
422 does not prohibit the occurrence of volcanic activity, if the influx of unradiogenic Os
423 from volcanism was outweighed by radiogenic Os input from weathering of the
424 continental crust, as is thought to be the case for the Toarcian Ocean Anoxic Event
425 (Cohen et al., 2004; Percival et al., 2016; Kemp et al., 2020; Them et al., 2017), and
426 potentially the PETM to some degree (Ravizza et al., 2001; Dickson et al., 2015).

427 Whilst not supported by the coronene index and the lack of a negative $\delta^{13}\text{C}$
428 excursion, sill intrusion is still a possible scenario that would leave the majority of
429 igneous unit underground. Such a process could have allowed Hg to be emitted without
430 exposing massive mafic rock onto the Earth surface that could have been weathered to
431 deliver large amounts of unradiogenic osmium into the ocean (Dickson et al., 2015; Liu
432 et al., 2019a; Wieczorek et al., 2013). An impact scenario has also been proposed for
433 the F–F interval (e.g., Claeys et al., 1992). However, current Os isotope data do not
434 show any unradiogenic excursion that may support an impact scenario, and even if an

435 impact event occurred, the impactor is likely to have a very small size that leaves little
436 geochemical trace in the sedimentary record (Harris et al., 2013; Liu et al., 2020a;
437 Percival et al., 2019; Turgeon et al., 2007). Further studies about the timing, locality
438 and scale of proposed large igneous provinces are needed to fully understand the role
439 of large igneous provinces in the climate change and mass extinction of Late Devonian.

440

441 *5.3 Implications for the link between volcanism and the F–F mass extinction*

442 Whilst volcanism has been inferred as the cause of the Frasnian–Famennian mass
443 extinction on the basis of Hg spikes at several sections around the world, it is clear that
444 these enrichments are not documented in all locations (Estrada et al., 2018; Moreno et
445 al., 2018; Racki et al., 2020; Racki et al., 2018a; Racki et al., 2018b; Kaiho et al., 2021;
446 this study), arguing against a global-scale disturbance of the mercury cycle. Even where
447 Hg spikes are preserved, there is no consistency regarding their stratigraphic correlation.
448 Mercury enrichments are detected below, at and above the F–F boundary (e.g., Kaiho
449 et al., 2021; Racki, 2020 and references therein, H-32 core in this study). In addition,
450 several LIPs (e.g., Viluy Traps, Kola, Vyatka, and Pripyat-Dniepr-Donets rift systems;
451 Arzamastsev et al., 2017; Kiselev et al., 2006; Kravchinsky, 2012) were active during
452 the F–F period. Thus, even if the previously observed Hg anomalies were derived from
453 volcanism, it remains unclear whether they were sourced from a single volcanic system
454 or a combination of the LIPs, or an intensification in arc volcanism.

455 Further studies are needed to rigorously test the link between Hg and volcanism
456 during the F–F interval, especially the relative timing of sedimentary Hg enrichment
457 and F–F mass extinction (see e.g., Percival et al. 2018a). Moreover, high-resolution
458 geochronology work that can precisely characterize the eruption/magmatic history of
459 the LIPs is necessary to fully understand the role of volcanism in driving the climatic
460 and biotic changes during the F–F period (following the approaches undertaken for the
461 P–T mass extinction and Siberian traps, and T–J mass extinction and Central Atlantic
462 Province; e.g., Burgess et al., 2017; Davies et al., 2017).

463

464 **6. Conclusions**

465 Mercury records of six Upper Devonian sections from North America show no
466 sign of Hg enrichment associated with the F–F mass extinction (Fig. 2 and 3). Minor
467 Hg variations in the New York records are more likely to be controlled by a
468 combination of local deposition processes such as redox variation, organic matter
469 preservation, sulphide precipitation and clay mineral input, rather than perturbations by
470 volcanic events. Previous study of the New York sections suggests enhanced wildfire
471 activity (as evidenced by inertinite abundance) across the F–F interval. The lack of
472 correlation between inertinite abundance and Hg concentration data excludes wildfires
473 as a major source of Hg during the F–F transition interval, at least to North American
474 basins. These findings may indicate that during the F–F extinction, ash and charcoal
475 had low Hg contents, or that the wildfires were limited in scale and/or had low burning

476 severity that released minimum Hg into the local environment. The H-32 section (Iowa)
477 records a possible volcanism-driven Hg enrichment with coeval increase of TOC
478 values; however, this Hg anomaly is stratigraphically above the F–F boundary (Fig. 3).
479 A volcanic trigger for the F–F mass extinction has recently been supported by Hg
480 anomalies data from widespread localities, but is not reinforced by study of the North
481 American F–F archives investigated here. Further investigations are needed to
482 understand why some F–F records are marked by pronounced Hg peaks, and others not,
483 as well as the timing and scale of Late Devonian volcanism and its potential role in
484 driving the F–F biotic crisis.

485

486 **Acknowledgements**

487 We thank Jin Si Over for field assistance in collecting the New York outcrop
488 sections. Brian Slater at the New York State Museum is thanked for facilitating the
489 collection of the WV core samples, and Jed Day and the Iowa Geological Survey for
490 access to the H-32 core. David Verstraeten and Christophe Snoeck are thanked for
491 assistance with laboratory analyses. We gratefully acknowledge the TOTAL
492 Endowment Fund and the CUG Wuhan Dida Scholarship to DS, the Flanders Research
493 Foundation (FWO: grant no 12P4519N), and Vrije Universiteit Brussel to LMEP and
494 the University of Durham, China Scholarship Council, China Postdoctoral Science
495 Foundation and Guangzhou Institute of Geochemistry to ZL.

496 **References**

497 Algeo, T.J., Berner, R.A., Maynard, J.B., Scheckler, S.E., 1995. Late Devonian oceanic
498 anoxic events and biotic crises: “rooted” in the evolution of vascular land plants.
499 GSA today 5, 45.

500 Algeo, T.J., 2004. Can marine anoxic events draw down the trace element inventory of
501 seawater? *Geology* 32, 1057-1060.

502 Algeo, T.J., Liu, J., 2020. A re-assessment of elemental proxies for paleoredox analysis.
503 *Chemical Geology* 540, 119549.

504 Amos, H.M., Jacob, D.J., Kocman, D., Horowitz, H.M., Zhang, Y., Dutkiewicz, S.,
505 Horvat, M., Corbitt, E.S., Krabbenhoft, D.P., Sunderland, E.M., 2014. Global
506 Biogeochemical Implications of Mercury Discharges from Rivers and Sediment
507 Burial. *Environmental Science & Technology* 48, 9514-9522.

508 Arzamastsev, A.A., Vesolovskiy, R.V., Travin, A.V., Yudin, D.S., Belyatsky, B.V.,
509 2017. Paleozoic tholeiitic magmatism of the Kola province: Spatial distribution,
510 age, and relation to alkaline magmatism. *Petrology* 25, 42-65.

511 Becker, R.T., Gradstein, F.M., Hammer, O., 2012. Chapter 22 - The Devonian Period,
512 in: Gradstein, F.M., Ogg, J.G., Schmitz, M.D., Ogg, G.M. (Eds.), *The Geologic*
513 *Time Scale*. Elsevier, Boston, pp. 559-601.

514 Bergquist, B.A., 2017. Mercury, volcanism, and mass extinctions. *Proceedings of the*
515 *National Academy of Sciences* 114, 8675-8677.

516 Biester, H., Scholz, C., 1996. Determination of Mercury Binding Forms in
517 Contaminated Soils: Mercury Pyrolysis versus Sequential Extractions.
518 *Environmental Science & Technology* 31, 233-239.

519 Biswas, A., Blum, J.D., Keeler, G.J., 2008. Mercury storage in surface soils in a central
520 Washington forest and estimated release during the 2001 Rex Creek Fire. *Science*
521 *of The Total Environment* 404, 129-138.

522 Biswas, A., Blum, J.D., Klaue, B., Keeler, G.J., 2007. Release of mercury from Rocky
523 Mountain forest fires. *Global Biogeochemical Cycles* 21.

524 Bond, D., Wignall, P.B., Racki, G., 2004. Extent and duration of marine anoxia during
525 the Frasnian–Famennian (Late Devonian) mass extinction in Poland, Germany,
526 Austria and France. *Geological Magazine* 141, 173-193.

527 Bond, D.P.G., Wignall, P.B., 2008. The role of sea-level change and marine anoxia in
528 the Frasnian–Famennian (Late Devonian) mass extinction. *Palaeogeography,*
529 *Palaeoclimatology, Palaeoecology* 263, 107-118.

530 Boudinot, F.G., Sepúlveda, J., 2020. Marine organic carbon burial increased forest fire
531 frequency during Oceanic Anoxic Event 2. *Nature Geoscience* 13, 693-698.

532 Burgess, S. D., Muirhead, J. D., and Bowring, S. A., 2017, Initial pulse of Siberian
533 Traps sills as the trigger of the end-Permian mass extinction: *Nature*
534 *Communications* 8, 164.

535 Charbonnier, G., Föllmi, K.B., 2017. Mercury enrichments in lower Aptian sediments
536 support the link between Ontong Java large igneous province activity and oceanic
537 anoxic episode 1a. *Geology* 45, 63-66.

538 Chester, R., 1990. The transport of material to the oceans: Relative flux magnitudes,
539 Marine Geochemistry. Springer, pp. 149-191.

540 Chen, D., Qing, H., Li, R., 2005. The Late Devonian Frasnian–Famennian (F/F) biotic
541 crisis: Insights from $\delta^{13}\text{C}_{\text{carb}}$, $\delta^{13}\text{C}_{\text{org}}$ and $^{87}\text{Sr}/^{86}\text{Sr}$ isotopic systematics. Earth and
542 Planetary Science Letters 235, 151-166.

543 Claeys, P., Casier, J.-G., Margolis, S.V., 1992. Microtektites and Mass Extinctions:
544 Evidence for a Late Devonian Asteroid Impact. Science 257, 1102-1104.

545 Cohen, A.S., Coe, A.L., 2002. New geochemical evidence for the onset of volcanism
546 in the Central Atlantic magmatic province and environmental change at the
547 Triassic-Jurassic boundary. Geology 30, 267-270.

548 Cohen, A.S., Coe, A.L., Harding, S.M., Schwark, L., 2004. Osmium isotope evidence
549 for the regulation of atmospheric CO_2 by continental weathering. Geology 32,
550 157-160.

551 Courtillot, V., Kravchinsky, V.A., Quidelleur, X., Renne, P.R., Gladkochub, D.P., 2010.
552 Preliminary dating of the Viluy traps (Eastern Siberia): Eruption at the time of
553 Late Devonian extinction events? Earth and Planetary Science Letters 300, 239-
554 245.

555 Da Silva, A.-C., Sinnesael, M., Claeys, P., Davies, J.H.F.L., de Winter, N.J., Percival,
556 L.M.E., Schaltegger, U., De Vleeschouwer, D., 2020. Anchoring the Late
557 Devonian mass extinction in absolute time by integrating climatic controls and
558 radio-isotopic dating. Scientific Reports 10, 12940.

559 Davies, J.H.F.L., Marzoli, A., Bertrand, H., Youbi, N., Ernesto, M., Schaltegger, U.,
560 2017. End-Triassic mass extinction started by intrusive CAMP activity. Nature
561 Communications 8, 15596.

562 Day, J., Witzke, B.J., 2017. Chapter Six - Upper Devonian Biostratigraphy, Event
563 Stratigraphy, and Late Frasnian Kellwasser Extinction Bioevents in the Iowa
564 Basin: Western Euramerica, in: Montenari, M. (Ed.), Stratigraphy & Timescales.
565 Academic Press, pp. 243-332.

566 De Vleeschouwer, D., Da Silva, A.-C., Sinnesael, M., Chen, D., Day, J.E., Whalen,
567 M.T., Guo, Z., Claeys, P., 2017. Timing and pacing of the Late Devonian mass
568 extinction event regulated by eccentricity and obliquity. Nature Communications
569 8, 2268.

570 DeBano, L.F., 2000. The role of fire and soil heating on water repellency in wildland
571 environments: a review. Journal of Hydrology 231-232, 195-206.

572 Dickson, A.J., Cohen, A.S., Coe, A.L., Davies, M., Shcherbinina, E.A., Gavrillov, Y.O.,
573 2015. Evidence for weathering and volcanism during the PETM from Arctic
574 Ocean and Peri-Tethys osmium isotope records. Palaeogeography,
575 Palaeoclimatology, Palaeoecology 438, 300-307.

576 Driscoll, C.T., Mason, R.P., Chan, H.M., Jacob, D.J., Pirrone, N., 2013. Mercury as a
577 Global Pollutant: Sources, Pathways, and Effects. Environmental Science &
578 Technology 47, 4967-4983.

- 579 Du Vivier, A.D.C., Selby, D., Sageman, B.B., Jarvis, I., Gröcke, D.R., Voigt, S., 2014.
580 Marine $^{187}\text{Os}/^{188}\text{Os}$ isotope stratigraphy reveals the interaction of volcanism and
581 ocean circulation during Oceanic Anoxic Event 2. *Earth and Planetary Science*
582 *Letters* 389, 23-33.
- 583 Du Vivier, A.D.C., Selby, D., Condon, D.J., Takashima, R., Nishi, H., 2015. Pacific
584 $^{187}\text{Os}/^{188}\text{Os}$ isotope chemistry and U–Pb geochronology: Synchronicity of global
585 Os isotope change across OAE 2. *Earth and Planetary Science Letters* 428, 204-
586 216.
- 587 Estrada, L., Pippenger, K., Boyer, D.L., Jones, D.S., Cohen, P., 2018. Mercury and
588 microfossil trends during end-Devonian extinction events, GSA Annual Meeting
589 in Indianapolis, Indiana, USA-2018. GSA.
- 590 Fisher, J.A., Jacob, D.J., Soerensen, A.L., Amos, H.M., Steffen, A., Sunderland, E.M.,
591 2012. Riverine source of Arctic Ocean mercury inferred from atmospheric
592 observations. *Nature Geoscience* 5, 499-504.
- 593 Friedli, H.R., Radke, L.F., Prescott, R., Hobbs, P.V., Sinha, P., 2003. Mercury
594 emissions from the August 2001 wildfires in Washington State and an agricultural
595 waste fire in Oregon and atmospheric mercury budget estimates. *Global*
596 *Biogeochemical Cycles* 17.
- 597 Gamboa Ruiz, W.L., Tomiyasu, T., 2015. Distribution of mercury in sediments from
598 Kagoshima Bay, Japan, and its relationship with physical and chemical factors.
599 *Environmental Earth Sciences* 74, 1175-1188.
- 600 Gehrke, G.E., Blum, J.D., Meyers, P.A., 2009. The geochemical behavior and isotopic
601 composition of Hg in a mid-Pleistocene western Mediterranean sapropel.
602 *Geochimica et Cosmochimica Acta* 73, 1651-1665.
- 603 Georgiev, S.V., Stein, H.J., Hannah, J.L., Henderson, C.M., Algeo, T.J., 2015.
604 Enhanced recycling of organic matter and Os-isotopic evidence for multiple
605 magmatic or meteoritic inputs to the Late Permian Panthalassic Ocean, Opal Creek,
606 Canada. *Geochimica et Cosmochimica Acta* 150, 192-210.
- 607 Glasspool, I.J., Scott, A.C., 2010. Phanerozoic concentrations of atmospheric oxygen
608 reconstructed from sedimentary charcoal. *Nature Geoscience* 3, 627.
- 609 Gordon, G.W., Rockman, M., Turekian, K.K., Over, J., 2009. Osmium isotopic
610 evidence against an impact at the Frasnian-Famennian boundary. 309, 420-430.
- 611 Grasby, S.E., Beauchamp, B., Bond, D.P.G., Wignall, P.B., Sanei, H., 2016. Mercury
612 anomalies associated with three extinction events (Capitanian Crisis, Latest
613 Permian Extinction and the Smithian/Spathian Extinction) in NW Pangea.
614 *Geological Magazine* 153, 285-297.
- 615 Grasby, S.E., Liu, X., Yin, R., Ernst, R.E., Chen, Z., 2020. Toxic mercury pulses into
616 late Permian terrestrial and marine environments. *Geology*.
- 617 Grasby, S.E., Sanei, H., Beauchamp, B., Chen, Z., 2013. Mercury deposition through
618 the Permo–Triassic Biotic Crisis. *Chemical Geology* 351, 209-216.

619 Grasby, S.E., Shen, W., Yin, R., Gleason, J.D., Blum, J.D., Lepak, R.F., Hurley, J.P.,
620 Beauchamp, B., 2017. Isotopic signatures of mercury contamination in latest
621 Permian oceans. *Geology* 45, 55-58.

622 Grasby, S.E., Them, T.R., Chen, Z., Yin, R., Ardakani, O.H., 2019. Mercury as a proxy
623 for volcanic emissions in the geologic record. *Earth-Science Reviews* 196, 102880.

624 Huang, C., Joachimski, M.M., Gong, Y., 2018. Did climate changes trigger the Late
625 Devonian Kellwasser Crisis? Evidence from a high-resolution conodont $\delta^{18}\text{OPO}_4$
626 record from South China. *Earth and Planetary Science Letters* 495, 174-184.

627 Joachimski, M.M., Breisig, S., Buggisch, W., Talent, J.A., Mawson, R., Gereke, M.,
628 Morrow, J.R., Day, J., Weddige, K., 2009. Devonian climate and reef evolution:
629 Insights from oxygen isotopes in apatite. *Earth and Planetary Science Letters* 284,
630 599-609.

631 Joachimski, M.M., Buggisch, W., 1993. Anoxic events in the late Frasnian—Causes of
632 the Frasnian-Famennian faunal crisis? *Geology* 21, 675-678.

633 Joachimski, M.M., Buggisch, W., 2002. Conodont apatite $\delta^{18}\text{O}$ signatures indicate
634 climatic cooling as a trigger of the Late Devonian mass extinction. *Geology* 30,
635 711-714.

636 Joachimski, M.M., Pancost, R.D., Freeman, K.H., Ostertag-Henning, C., Buggisch, W.,
637 2002. Carbon isotope geochemistry of the Frasnian–Famennian transition.
638 *Palaeogeography, Palaeoclimatology, Palaeoecology* 181, 91-109.

639 Johnson, J.G., Klapper, G., Sandberg, C.A., 1985. Devonian Eustatic Fluctuations in
640 Euramerica. *Geological Society of America Bulletin* 96, 567-587.

641 Jones, M.T., Percival, L.M.E., Stokke, E.W., Frieling, J., Mather, T.A., Riber, L.,
642 Schubert, B.A., Schultz, B., Tegner, C., Planke, S., Svensen, H.H., 2018. Mercury
643 anomalies across the Palaeocene-Eocene Thermal Maximum. *Clim. Past Discuss.*
644 2018, 1-35.

645 Kaiho, K., Aftabuzzaman, M., Jones, D.S., Tian, L., 2020. Pulsed volcanic combustion
646 events coincident with the end-Permian terrestrial disturbance and the following
647 global crisis. *Geology* 49, 289-293.

648 Kaiho, K., Miura, M., Tezuka, M., Hayashi, N., Jones, D.S., Oikawa, K., Casier, J.-G.,
649 Fujibayashi, M., Chen, Z.-Q., 2021. Coronene, mercury, and biomarker data
650 support a link between extinction magnitude and volcanic intensity in the Late
651 Devonian. *Global and Planetary Change* 199, 103452.

652 Kaiho, K., Oshima, N., Adachi, K., Adachi, Y., Mizukami, T., Fujibayashi, M., Saito,
653 R., 2016. Global climate change driven by soot at the K-Pg boundary as the cause
654 of the mass extinction. *Scientific Reports* 6, 28427.

655 Kemp, D.B., Selby, D., Izumi, K., 2020. Direct coupling between carbon release and
656 weathering during the Toarcian oceanic anoxic event. *Geology*.

657 Kiselev, A.I., Yarmolyuk, V.V., Egorov, K.N., Chernyshov, R.A., Nikiforov, A.V.,
658 2006. Middle Paleozoic basic magmatism of the northwestern Vilyui Rift:
659 Composition, sources, and geodynamics. *Petrology* 14, 588-608.

660 Klapper, G., Feist, R., Becker, R.T., House, M.R., 1993. Definition of the Frasnian
661 Famennian Stage Boundary. *Episodes* 16, 433-441.

662 Kravchinsky, V.A., 2012. Paleozoic large igneous provinces of Northern Eurasia:
663 Correlation with mass extinction events. *Global and Planetary Change* 86-87, 31-
664 36.

665 Kuroda, J., Hori, R.S., Suzuki, K., Gröcke, D.R., Ohkouchi, N., 2010. Marine osmium
666 isotope record across the Triassic-Jurassic boundary from a Pacific pelagic site.
667 *Geology* 38, 1095-1098.

668 Lima, A.L.C., Farrington, J.W., Reddy, C.M., 2005. Combustion-Derived Polycyclic
669 Aromatic Hydrocarbons in the Environment—A Review. *Environmental*
670 *Forensics* 6, 109-131.

671 Liu, Z., Horton, D.E., Tabor, C., Sageman, B.B., Percival, L.M.E., Gill, B.C., Selby,
672 D., 2019a. Assessing the Contributions of Comet Impact and Volcanism Toward
673 the Climate Perturbations of the Paleocene-Eocene Thermal Maximum.
674 *Geophysical Research Letters* 46, 14798-14806.

675 Liu, Z., Selby, D., Hackley, P.C., Over, D.J., 2020a. Evidence of wildfires and elevated
676 atmospheric oxygen at the Frasnian–Famennian boundary in New York (USA):
677 Implications for the Late Devonian mass extinction. *GSA Bulletin*.

678 Liu, Z., Selby, D., Zhang, H., Shen, S., 2020b. Evidence for volcanism and weathering
679 during the Permian-Triassic mass extinction from Meishan (South China) osmium
680 isotope record. *Palaeogeography, Palaeoclimatology, Palaeoecology* 553, 109790.

681 Liu, Z., Selby, D., Zhang, H., Zheng, Q., Shen, S., Sageman, B.B., Grasby, S.E.,
682 Beauchamp, B., 2019b. Osmium-isotope evidence for volcanism across the
683 Wuchiapingian–Changhsingian boundary interval. *Chemical Geology* 529,
684 119313.

685 McElwain, J.C., Wade-Murphy, J., Hesselbo, S.P., 2005. Changes in carbon dioxide
686 during an oceanic anoxic event linked to intrusion into Gondwana coals. *Nature*
687 435, 479-482.

688 Moreno, C., González, F., Sáez, R., Melgarejo, J.C., Suárez-Ruiz, I., 2018. The Upper
689 Devonian Kellwasser event recorded in a regressive sequence from inner shelf to
690 lagoonal pond, Catalan Coastal Ranges, Spain. *Sedimentology* 65, 2055-2087.

691 Obrist, D., 2007. Atmospheric mercury pollution due to losses of terrestrial carbon
692 pools? *Biogeochemistry* 85, 119-123.

693 Obrist, D., Kirk, J.L., Zhang, L., Sunderland, E.M., Jiskra, M., Selin, N.E., 2018. A
694 review of global environmental mercury processes in response to human and
695 natural perturbations: Changes of emissions, climate, and land use. *Ambio* 47,
696 116-140.

697 Outridge, Sanei, H., Stern, Hamilton, Goodarzi, F., 2007. Evidence for Control of
698 Mercury Accumulation Rates in Canadian High Arctic Lake Sediments by
699 Variations of Aquatic Primary Productivity. *Environmental Science &*
700 *Technology* 41, 5259-5265.

701 Over, D.J., 1997. Conodont biostratigraphy of the Java Formation (Upper Devonian)
702 and the Frasnian-Famennian boundary in western New York State, in: Klapper,
703 G., Murphy, M.A., Talent, J.A. (Eds.), *Paleozoic Sequence Stratigraphy,*
704 *Biostratigraphy, and Biogeography: Studies in Honor of J. Granville ("Jess")*
705 *Johnson.* Geological Society of America, pp. 161-177.

706 Over, D.J., 2002. The Frasnian/Famennian boundary in central and eastern United
707 States. *Palaeogeography, Palaeoclimatology, Palaeoecology* 181, 153-169.

708 Paschall, O., Carmichael, S.K., Königshof, P., Waters, J.A., Ta, P.H., Komatsu, T.,
709 Dombrowski, A., 2019. The Devonian-Carboniferous boundary in Vietnam:
710 Sustained ocean anoxia with a volcanic trigger for the Hangenberg Crisis? *Global*
711 *and Planetary Change* 175, 64-81.

712 Percival, L.M.E., van Helmond, N.A.G.M., Selby, D., Goderis, S., Claeys, P., 2020.
713 Complex Interactions Between Large Igneous Province Emplacement and Global-
714 Temperature Changes During the Cenomanian-Turonian Oceanic Anoxic Event
715 (OAE 2). *Paleoceanography and Paleoclimatology* 35, e2020PA004016.

716 Percival, L.M.E., Cohen, A.S., Davies, M.K., Dickson, A.J., Hesselbo, S.P., Jenkyns,
717 H.C., Leng, M.J., Mather, T.A., Storm, M.S., Xu, W., 2016. Osmium isotope
718 evidence for two pulses of increased continental weathering linked to Early
719 Jurassic volcanism and climate change. *Geology* 44, 759-762.

720 Percival, L.M.E., Davies, J.H.F.L., Schaltegger, U., De Vleeschouwer, D., Da Silva,
721 A.C., Föllmi, K.B., 2018a. Precisely dating the Frasnian–Famennian boundary:
722 implications for the cause of the Late Devonian mass extinction. *Scientific Reports*
723 8, 9578.

724 Percival, L.M.E., Jenkyns, H.C., Mather, T.A., Dickson, A.J., Batenburg, S.J., Ruhl,
725 M., Hesselbo, S.P., Barclay, R., Jarvis, I., Robinson, S.A., Woelders, L., 2018b.
726 Does large igneous province volcanism always perturb the mercury cycle?
727 Comparing the records of Oceanic Anoxic Event 2 and the end-Cretaceous to other
728 Mesozoic events. *American Journal of Science* 318, 799-860.

729 Percival, L.M.E., Ruhl, M., Hesselbo, S.P., Jenkyns, H.C., Mather, T.A., Whiteside,
730 J.H., 2017. Mercury evidence for pulsed volcanism during the end-Triassic mass
731 extinction. *Proceedings of the National Academy of Sciences* 114, 7929-7934.

732 Percival, L.M.E., Selby, D., Bond, D.P.G., Rakociński, M., Racki, G., Marynowski, L.,
733 Adatte, T., Spangenberg, J.E., Föllmi, K.B., 2019. Pulses of enhanced continental
734 weathering associated with multiple Late Devonian climate perturbations:
735 Evidence from osmium-isotope compositions. *Palaeogeography,*
736 *Palaeoclimatology, Palaeoecology.*

737 Percival, L.M.E., Witt, M.L.I., Mather, T.A., Hermoso, M., Jenkyns, H.C., Hesselbo,
738 S.P., Al-Suwaidi, A.H., Storm, M.S., Xu, W., Ruhl, M., 2015. Globally enhanced
739 mercury deposition during the end-Pliensbachian extinction and Toarcian OAE:
740 A link to the Karoo–Ferrar Large Igneous Province. *Earth and Planetary Science*
741 *Letters* 428, 267-280.

742 Percival, L.M.E., Marynowski, L., Baudin, F., Goderis, S., De Vleeschouwer, D.,
743 Rakociński, M., Narkiewicz, K., Da Silva, A.-C. and Claeys, P., Regional
744 variability in the timing and nature of environmental perturbations during the
745 Frasnian–Famennian mass extinction. (in review)

746 Peucker-Ehrenbrink, B., Ravizza, G., 2000. The marine osmium isotope record. *Terra*
747 *Nova* 12, 205-219.

748 Peucker-Ehrenbrink, B., Ravizza, G., 2012. Osmium Isotope Stratigraphy, in:
749 Gradstein, F.M., Ogg, J.G., Schmitz, M.D., Ogg, G.M. (Eds.), *The Geologic Time*
750 *Scale*. Elsevier, Boston, pp. 145-166.

751 Racki, G., 2020. A volcanic scenario for the Frasnian–Famennian major biotic crisis
752 and other Late Devonian global changes: More answers than questions? *Global*
753 *and Planetary Change* 189, 103174.

754 Racki, G., Adatte, T., Bond, D.P.G., Keller, G., 2020. Volcanism as a prime cause of
755 mass extinctions: Retrospectives and perspectives, *Mass Extinctions, Volcanism,*
756 *and Impacts: New Developments*. Geological Society of America, p. 0.

757 Racki, G., Königshof, P., Belka, Z., Dopieralska, J., Piszczowska, A., 2019. Diverse
758 depositional and geochemical signatures of the Frasnian-Famennian global event
759 in western Thailand reveal palaeotethyan vs. Western Australian geotectonic
760 affinities. *Journal of Asian Earth Sciences: X* 2, 100010.

761 Racki, G., Racka, M., Matyja, H., Devleeschouwer, X., 2002. The Frasnian/Famennian
762 boundary interval in the South Polish–Moravian shelf basins: integrated event-
763 stratigraphical approach. *Palaeogeography, Palaeoclimatology, Palaeoecology*
764 181, 251-297.

765 Racki, G., Rakociński, M., Marynowski, L., 2018a. Anomalous Upper Devonian
766 mercury enrichments: comparison of Inductively Coupled Plasma – Mass
767 Spectrometry (ICP-MS) and Atomic Absorption Spectrometry (AAS) analytical
768 data. 2018 62.

769 Racki, G., Rakociński, M., Marynowski, L., Wignall, P.B., 2018b. Mercury
770 enrichments and the Frasnian-Famennian biotic crisis: A volcanic trigger proved?
771 *Geology* 46, 543-546.

772 Rakociński, M., Marynowski, L., Piszczowska, A., Bełdowski, J., Siedlewicz, G., Zatoń,
773 M., Perri, M.C., Spalletta, C., Schönlaub, H.P., 2020. Volcanic related
774 methylmercury poisoning as the possible driver of the end-Devonian Mass
775 Extinction. *Scientific Reports* 10, 7344.

776 Sageman, B.B., Murphy, A.E., Werne, J.P., Ver Straeten, C.A., Hollander, D.J., Lyons,
777 T.W., 2003. A tale of shales: the relative roles of production, decomposition, and
778 dilution in the accumulation of organic-rich strata, Middle–Upper Devonian,
779 Appalachian basin. *Chemical Geology* 195, 229-273.

780 Sanei, H., Grasby, S.E., Beauchamp, B., 2012. Latest Permian mercury anomalies.
781 *Geology* 40, 63-66.

782 Sanei, H., Outridge, P.M., Stern, G.A., Macdonald, R.W., 2014. Classification of
783 mercury–labile organic matter relationships in lake sediments. *Chemical Geology*
784 373, 87-92.

785 Shen, J., Algeo, T.J., Chen, J., Planavsky, N.J., Feng, Q., Yu, J., Liu, J., 2019a. Mercury
786 in marine Ordovician/Silurian boundary sections of South China is sulfide-hosted
787 and non-volcanic in origin. *Earth and Planetary Science Letters* 511, 130-140.

788 Shen, J., Chen, J., Algeo, T.J., Yuan, S., Feng, Q., Yu, J., Zhou, L., O’Connell, B.,
789 Planavsky, N.J., 2019b. Evidence for a prolonged Permian–Triassic extinction
790 interval from global marine mercury records. *Nature Communications* 10, 1563.

791 Shen, J., Yu, J., Chen, J., Algeo, T.J., Xu, G., Feng, Q., Shi, X., Planavsky, N.J., Shu,
792 W., Xie, S., 2019. Mercury evidence of intense volcanic effects on land during the
793 Permian-Triassic transition. *Geology* 47, 1117-1121.

794 Shen, J., Feng, Q., Algeo, T.J., Liu, J., Zhou, C., Wei, W., Liu, J., Them, T.R., Gill,
795 B.C., Chen, J., 2020. Sedimentary host phases of mercury (Hg) and implications
796 for use of Hg as a volcanic proxy. *Earth and Planetary Science Letters* 543, 116333.

797 Sholupov, S.E., Ganeyev, A.A., 1995. Zeeman atomic absorption spectrometry using
798 high frequency modulated light polarization. *Spectrochimica Acta Part B: Atomic*
799 *Spectroscopy* 50, 1227-1236.

800 Song, Y., Gilleaudeau, G.J., Algeo, T.J., Over, D.J., Lyons, T.W., Anbar, A.D., Xie, S.,
801 2020. Biomarker evidence of algal-microbial community changes linked to redox
802 and salinity variation, Upper Devonian Chattanooga Shale (Tennessee, USA).
803 *GSA Bulletin*.

804 Song, H., Song, H., Algeo, T.J., Tong, J., Romaniello, S.J., Zhu, Y., Chu, D., Gong, Y.,
805 Anbar, A.D., 2017. Uranium and carbon isotopes document global-ocean redox-
806 productivity relationships linked to cooling during the Frasnian-Famennian mass
807 extinction. *Geology* 45, 887-890.

808 Soerensen, A.L., Jacob, D.J., Streets, D.G., Witt, M.L.I., Ebinghaus, R., Mason, R.P.,
809 Andersson, M., Sunderland, E.M., 2012. Multi-decadal decline of mercury in the
810 North Atlantic atmosphere explained by changing subsurface seawater
811 concentrations. *Geophysical Research Letters* 39.

812 Stanley, S.M., 2016. Estimates of the magnitudes of major marine mass extinctions in
813 earth history. *Proc Natl Acad Sci U S A* 113, E6325-E6334.

814 Stephens, N.P., Sumner, D.Y., 2003. Late Devonian carbon isotope stratigraphy and
815 sea level fluctuations, Canning Basin, Western Australia. *Palaeogeography,*
816 *Palaeoclimatology, Palaeoecology* 191, 203-219.

817 Svensen, H., Planke, S., Malthe-Sørensen, A., Jamtveit, B., Myklebust, R., Rasmussen
818 Eidem, T., Rey, S.S., 2004. Release of methane from a volcanic basin as a
819 mechanism for initial Eocene global warming. *Nature* 429, 542.

820 Svensen, H., Planke, S., Polozov, A.G., Schmidbauer, N., Corfu, F., Podladchikov,
821 Y.Y., Jamtveit, B., 2009. Siberian gas venting and the end-Permian environmental
822 crisis. *Earth and Planetary Science Letters* 277, 490-500.

823 Them, T.R., Gill, B.C., Selby, D., Gröcke, D.R., Friedman, R.M., Owens, J.D., 2017.
824 Evidence for rapid weathering response to climatic warming during the Toarcian
825 Oceanic Anoxic Event. *Scientific Reports* 7, 5003.

826 Them, T.R., Jagoe, C.H., Caruthers, A.H., Gill, B.C., Grasby, S.E., Gröcke, D.R., Yin,
827 R., Owens, J.D., 2019. Terrestrial sources as the primary delivery mechanism of
828 mercury to the oceans across the Toarcian Oceanic Anoxic Event (Early Jurassic).
829 *Earth and Planetary Science Letters* 507, 62-72.

830 Turgeon, S.C., Creaser, R.A., 2008. Cretaceous oceanic anoxic event 2 triggered by a
831 massive magmatic episode. *Nature* 454, 323-326.

832 Turgeon, S.C., Creaser, R.A., Algeo, T.J., 2007. Re–Os depositional ages and seawater
833 Os estimates for the Frasnian–Famennian boundary: Implications for weathering
834 rates, land plant evolution, and extinction mechanisms. *Earth and Planetary
835 Science Letters* 261, 649-661.

836 Wang, K., Geldsetzer, H.H.J., Goodfellow, W.D., Krouse, H.R., 1996. Carbon and
837 sulfur isotope anomalies across the Frasnian-Famennian extinction boundary,
838 Alberta, Canada. *Geology* 24, 187-191.

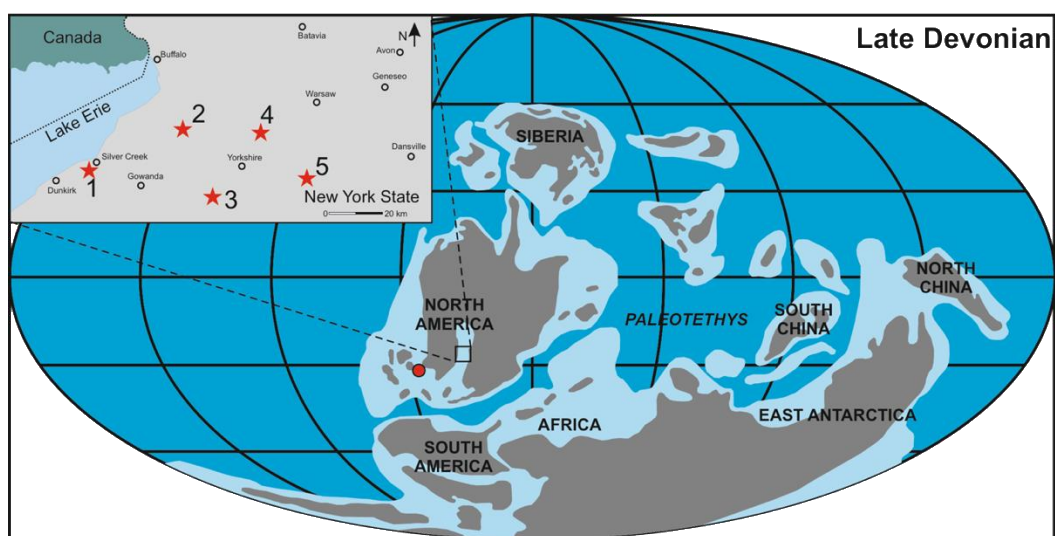
839 Webster, J.P., Kane, T.J., Obrist, D., Ryan, J.N., Aiken, G.R., 2016. Estimating mercury
840 emissions resulting from wildfire in forests of the Western United States. *Science
841 of The Total Environment* 568, 578-586.

842 Woodruff, L.G., Cannon, W.F., 2010. Immediate and Long-Term Fire Effects on Total
843 Mercury in Forests Soils of Northeastern Minnesota. *Environmental Science &
844 Technology* 44, 5371-5376.

845 Wieczorek, R., Fantle, M.S., Kump, L.R., Ravizza, G., 2013. Geochemical evidence
846 for volcanic activity prior to and enhanced terrestrial weathering during the
847 Paleocene Eocene Thermal Maximum. *Geochimica et Cosmochimica Acta* 119,
848 391-410.

849 **List of figures:**

850 **Figure 1.** Reconstructed paleogeography map showing location of the Appalachian
851 Basin (open square) and Illinois Basin (red circle) in North America, after Joachimski
852 et al. (2009). Inserted map showing present day New York sample locations – 1: Walnut
853 Creek Bank, 2: Irish Gulf, 3: West Valley, 4: Beaver Meadow Creek, 5: Joint Creek).

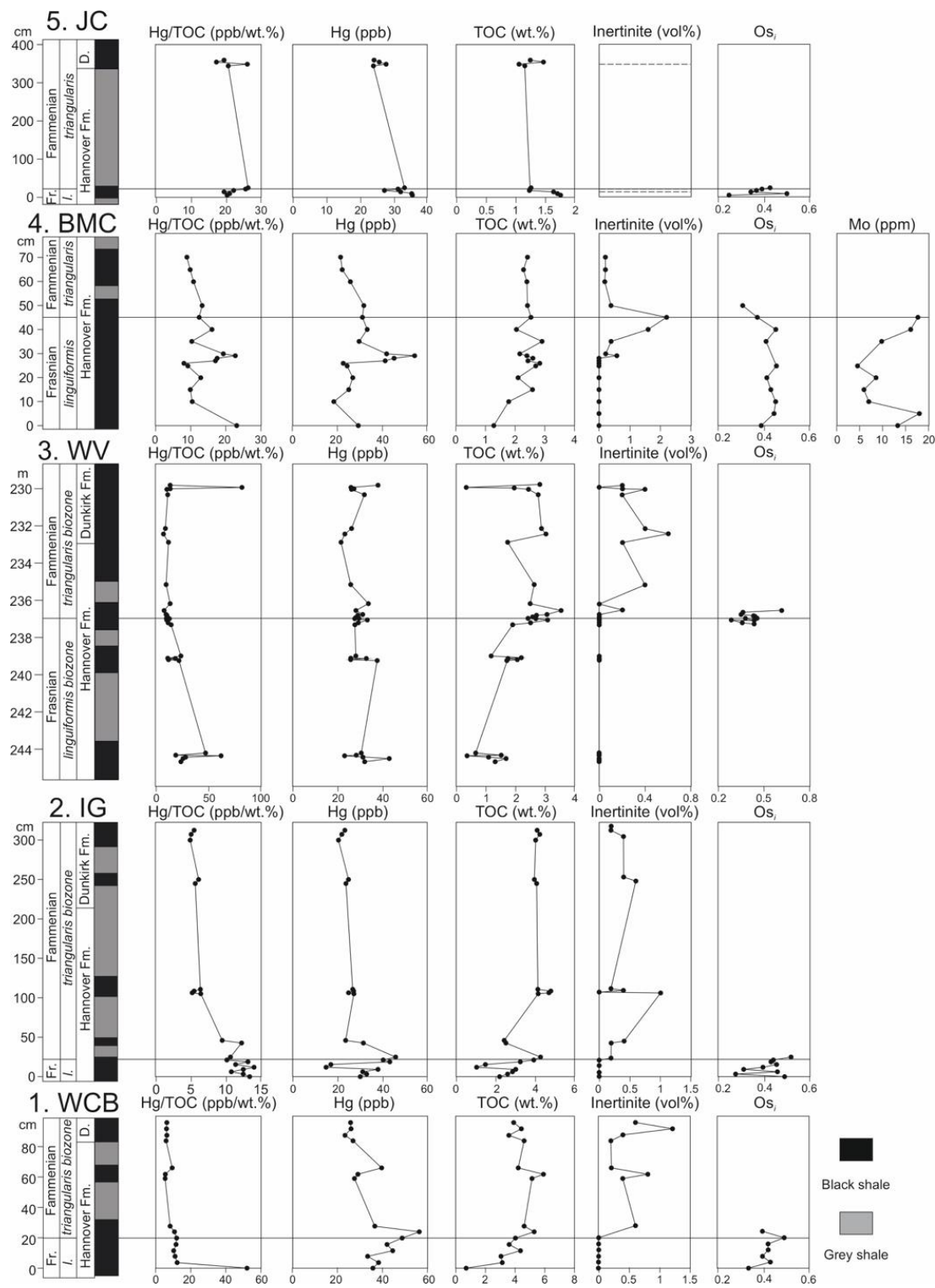


854

855 **Figure 2.** Hg and Hg/TOC stratigraphy for the New York sections investigated.

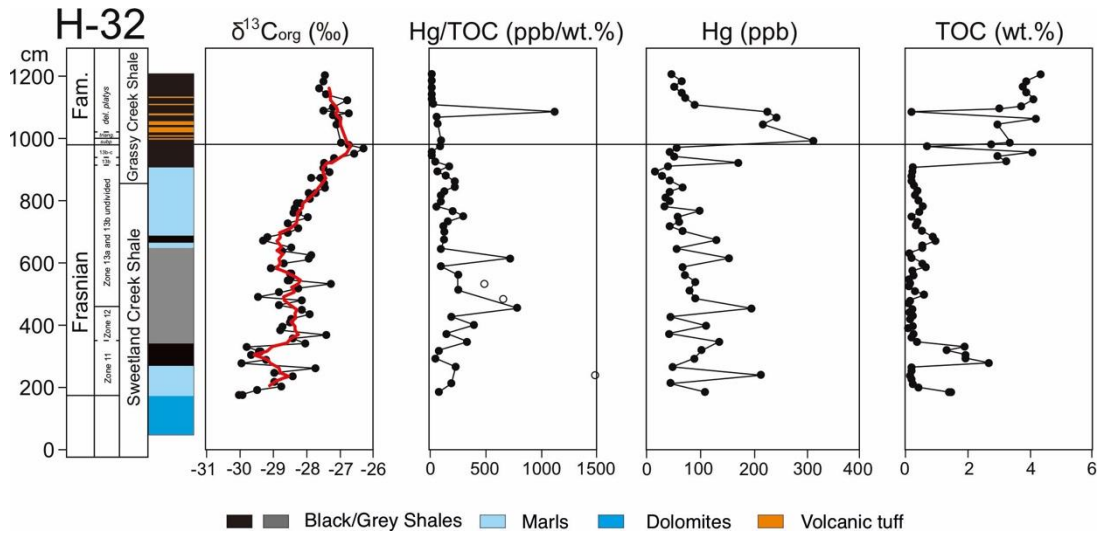
856 Inertinite data (volume percentage), Mo abundance and TOC data are from Liu et al.

857 (2020a).



858

859 **Figure 3.** Stratigraphic plot of $^{13}\text{C}_{\text{org}}$, Hg and Hg/TOC data for the H-32 section. $^{13}\text{C}_{\text{org}}$
 860 and TOC data are from Percival et al. (in review).

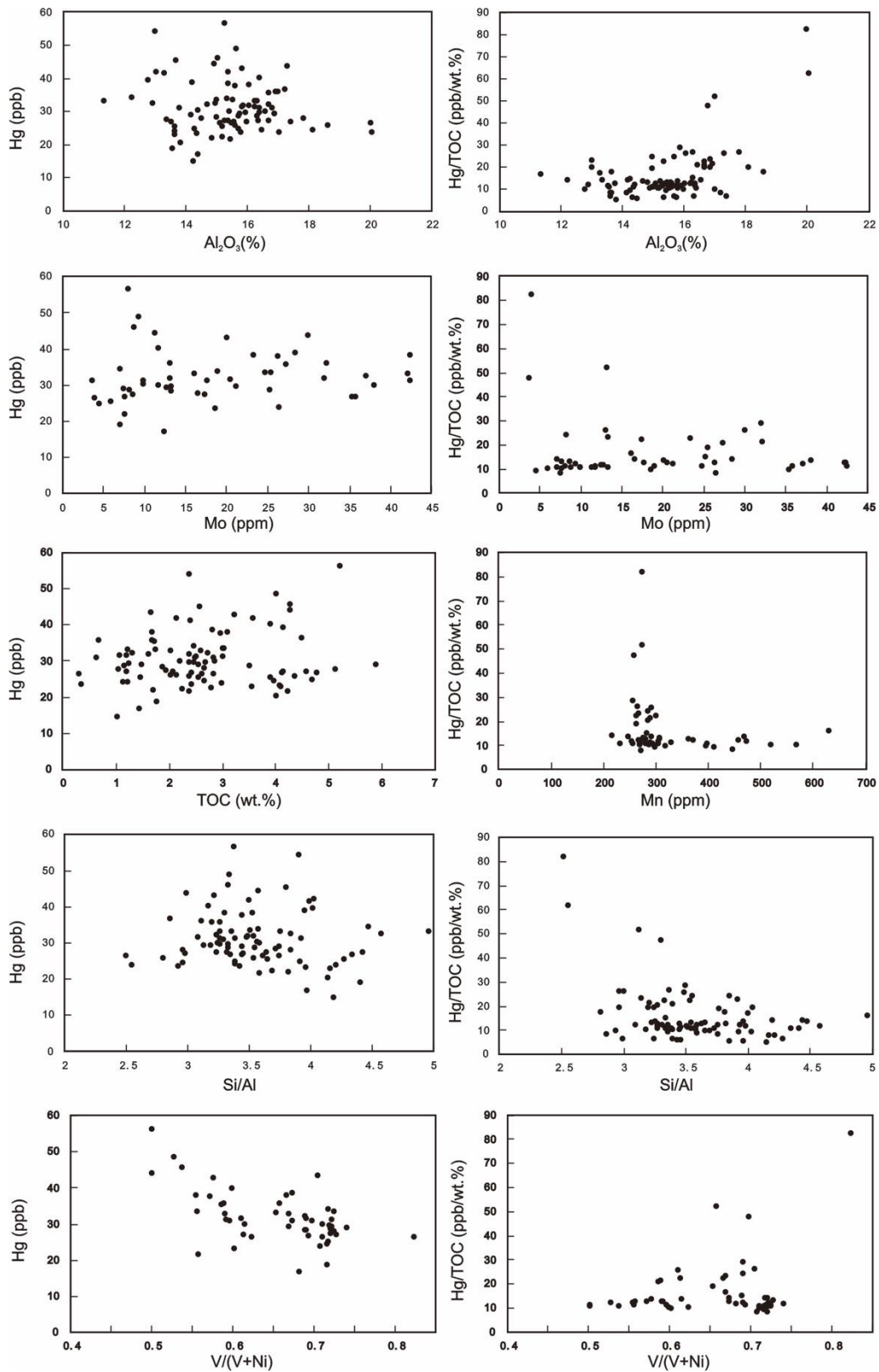


861

■ Black/Grey Shales ■ Marls ■ Dolomites ■ Volcanic tuff

862 **Figure 4.** Crossplots of Hg and Hg/TOC with TOC, Al₂O₃, Mo, Mn, V/(V+Ni) and

863 Si/Al.



864